

# A CASE STUDY OF UNSTEADY WINGS: THE WAKE OF A FREELY FLYING EUROPEAN STARLING (*STURNUS VULGARIS*)

**Adam J. Kirchhefer, Daniel Floryan**

Department of Mechanical and Materials Engineering,  
The University of Western Ontario  
London, Ontario, Canada  
akirchhe@uwo.ca, dfloryan@uwo.ca

**Wayne Bezner-Kerr, Chris G. Guglielmo**

Department of Biology,  
The University of Western Ontario  
London, Ontario, Canada  
wbezner@uwo.ca, cguglie2@uwo.ca

**Gregory A. Kopp**

Department of Civil and Environmental Engineering,  
The University of Western Ontario  
London, Ontario, Canada  
gakopp@uwo.ca

**Roi Gurka**

Department of Chemical Engineering,  
Ben-Gurion University  
Beer-sheva 84105, Israel  
gurka@bgu.ac.il

## ABSTRACT

The wake of a freely flying European Starling (*Sturnus Vulgaris*) is investigated as a case study of unsteady wing aerodynamics. Measurements of the wake have been taken using high speed particle image velocimetry and related to the bird's position in the wind tunnel. Regions of strong, negative, spanwise vorticity originating from the downstroke to upstroke transition have been found and characterized. Relatively strong vortices, defined based on vortex swirling strength, have been found at various streamwise locations. Smaller, weaker vortices from the downstroke have been found as well. To investigate wake dynamics, properties of the vorticity and vortices are considered over a range of streamwise positions spanning 4.4 to 6.3 average wing chords behind the wing root.

## INTRODUCTION

In recent years, an increasing interest in developing unmanned aerodynamic vehicles (UAVs) has prompted research on the related aerodynamic phenomena. This branch

of aerodynamics focuses on low Reynolds number wings, of a variety of shapes, moving unsteadily through a fluid. This unsteady motion generally leads to the creation of performance enhancing bound vortices on the lifting surface, which eventually detach, convect into the wake, and interact with other vortices (Rozhdestvensky and Ryzhov, 2003). Due to the interaction between the bound vortices on the lifting surface and the vortices in the wake, the performance of an unsteady wing is coupled with the formation and distribution of vorticity shed throughout the wing's cycle of oscillation (Dong et al., 2006; von Ellenrieder et al., 2008).

Traditionally, the studies in this field have been performed on well known geometries, such as NACA profile airfoils following, well defined sinusoidal trajectories of pitch and position (Anderson et al., 1998; Rozhdestvensky and Ryzhov, 2003). These motions are generally tested over a range of dimensionless parameters (Anderson et al., 1998). In addition to the Reynolds number, these parameters include the pitching amplitude, the dimensionless heaving amplitude, the Strouhal number, and the reduced frequency.

In the present work, the near wake of a freely flying European Starling (*Sturnus Vulgaris*) has been selected as a

case study of unsteady wing aerodynamics. Working with a live animal presents a difficulty in that the above parameters cannot be systematically tested. However, this also presents an opportunity. As living organisms, birds are subject to selective pressures. As such, one may assume they operate their wings in a manner that is highly efficient. Although this notion is supported by the tendency of birds, as well as many other animals, to operate in a Strouhal number range (0.2-0.4) of robustly high efficiency (Anderson et al., 1998; Taylor et al., 2003), there are many factors differentiating the flapping of a bird's wings from the heaving and pitching of two dimensional airfoils (von Ellenrieder et al., 2008). These differences include the presence of a body, the three dimensionality of the wing and the three dimensionality of its movement.

The goal of the present study is to investigate unsteady aerodynamics via analysis of the wake originating from the unsteady movement of the wings of a bird. The study focuses exclusively on the wake emanating from the transition from downstroke to upstroke at a spanwise location approximately halfway between the wing tip and the shoulder joint. The wake from this phase of the cycle typically contains relatively strong regions of spanwise vorticity originating from bound vortices on the wing (Hubel and Tropea, 2010; Rozhdestvensky and Ryzhov, 2003). Characterization of these regions of spanwise vorticity, over streamwise positions of 4.4 to 6.3 average wing chords behind the wing root, are presented and discussed.

## EXPERIMENTAL DETAILS

### Wind Tunnel

The experiment was performed in the hypobaric wind tunnel at the Advanced Facility for Avian Research (AFAR) at The University of Western Ontario. A plan view schematic of the experimental setup is seen in Figure 1. The octagonal test section, with a cross-sectional area of  $1.2 \text{ m}^2$ , is preceded by a 2:1 contraction. The width, height and length of the test section are 1 m, 1.5 m, and 2 m, respectively. An open jet exists between the downstream end of the test section and the diffuser. This opening is used for introducing the live bird to the wind tunnel during the experiment. The wind tunnel has turbulence intensity lower than 1.4% at the location where measurements were taken. A fine net was placed at the upstream end of the test section to prevent the bird from entering the contraction, and this did not alter the turbulence intensity significantly.

### Long-Duration Time-Resolved PIV System

Wake measurements were taken using the long-duration time-resolved PIV system developed at The University of Western Ontario (Taylor et al., 2010). Olive oil particles of a size of  $1 \mu\text{m}$  were introduced into the wind tunnel via a Laskin nozzle at the downstream end of the test section such that it would not cause a disturbance to the test section flow or to the

bird. Illumination of the flow field was provided by a light sheet formed from a 80 W, double-head, diode-pumped, Q-switched, Nd:YLF laser at a wavelength of 527nm. Performing at the highest available spatial resolution (1024 pixels by 1024 pixels), two cameras (Photron FASTCAM-1024PCI CMOS) recorded images at a rate of 1000 Hz. At this spatial resolution, the cameras are capable of acquiring images for 23 minutes continuously. One camera was used to record the position and wing beat cycle phase of the bird and the other was used for PIV. The PIV camera's field of view was approximately 12 cm by 12 cm in size ( $2c$  by  $2c$ ). Vector fields were generated using 32 pixel by 32 pixel interrogation windows with 50% overlap, giving a spatial resolution of 32 vectors per chord.

More detailed information regarding the system's components and capabilities are available in Taylor et al. (2010).

### The Bird: A European Starling

Wake measurements were taken from a European Starling that had been trained to fly in the AFAR wind tunnel. Based on the bird's ability to easily enter the wind tunnel through the shear of the open jet, the bird was used as an "instructor" for other birds.

The wings of the bird have an average chord,  $c$ , of 6 cm, a maximum wingspan,  $2b_{semi}$ , of 19.1 cm and an aspect ratio,  $AR$ , of 6.4. A typical cruising speed,  $U_\infty$ , of 12 m/s was chosen for the experiments. The cruising speed was chosen based on the bird's history of preferring to fly at this speed. The wing beat frequency,  $f$ , was 11.5 Hz. The wing tip vertical amplitude,  $A$ , was 26 cm. These quantities correspond to a chord based Reynolds number of 48,000, a Strouhal number ( $St=Af/U_\infty$ ) of 0.25 and a reduced frequency ( $k = \pi fc/U_\infty$ ) of 0.18. At the time the experiments were performed, the bird had a mass of 78 g and a lateral body width of 4 cm.

Due to the powerful laser operating within a few chord lengths of the bird's tail, two precautions were taken to ensure the bird's safety. Goggles made of a flexible, optically dense, polymer material were designed to protect the bird's vision as well as reduce the potential of the lightsheet frightening the bird. After an accommodation period in a cage of fifteen minutes to half an hour, the bird would fly normally in the tunnel while wearing the goggles.

To prevent direct contact between the bird and the light sheet, a collection of optoisolators operated by six infrared transceivers (Balluff Inc.) was integrated into the PIV system. The function of the optoisolators was to trigger the laser only when the bird was in a position upstream of the PIV field of view, slightly offset in the spanwise direction. An additional feature of having the laser triggered by the bird was that the images recorded by the PIV camera would only show the presence of a light sheet when the bird's wake coincident with the PIV field of view. During the experiment, 5,000 vector maps were recorded and 650 contain wake features. The set of 650 include sequences showing the convection of five regions of high spanwise vorticity through the field of view.

These sequences are referred to below as I through V, in order of upstream position to downstream position.

### The Bird's Position

The streamwise and vertical position of the bird for all measurements were recorded from one of the two 1000 Hz cameras. The field of view in these recordings has an area of  $9c$  by  $9c$  which includes the upstream edge of the PIV field of view.

The spanwise position of the bird was recorded from a floor mounted camera operating at 60 Hz. A normalized spanwise position was derived from each image by measuring the spanwise position of the centre of the bird's body and dividing it by the measured width of the bird's body. The floor mounted camera was not synchronized with the PIV system, therefore, the two time histories were synchronized manually based on the presence of light from the laser firing. Once synchronized, spanwise positions were assigned to the wake data captured at 500 Hz based on interpolation from the simultaneously recorded spanwise positions recorded at 60 Hz.

The continuous movement of the bird about the test section leads to a difficulty in the association of wake data with the simultaneously measured position of the bird (see Figure 2).. Consider a point of reference,  $x^*$ , moving at the same velocity as the free stream. At time  $t_1$ , this point of reference is coincident with the streamwise position of the bird's wing root. Although the bird interacts with this parcel of air at  $t_1$ , the measurement of the phenomena does not occur until  $t_2$ . At  $t_2$ , the bird has triggered the laser and therefore prompted measurement of the wake. Equivalently, the wake measured at a given point in time does not correspond to the location of the bird or the phase of the wing beat cycle in which it is simultaneously seen. As a result, careful treatment has been made in order to associate the streamwise and spanwise location of the bird with the measurements in the wake.

The coordinate system presented herein is based on a frame of reference convection time,  $\Delta t = t_2 - t_1$ , normalized by the wing beat period,  $\tau$ . The convection time  $\Delta\tau = \Delta t / \tau$ , indicates the time that elapses between  $x^*$  having the same streamwise position as the wing root and  $x^*$  having the same streamwise position as the upstream edge of the PIV field of view. Therefore, in the frame of reference of the PIV field of view if it were travelling at free stream speed through the wind tunnel, wake measurements are recorded  $\Delta\tau$  after the bird's wing root has left the upstream edge of the field of view.

Given that  $x^*$  is moving at the free stream speed, 12 m/s,  $\Delta\tau$  relates to the distance,  $\Delta x/c = \Delta\tau \cdot U_\infty/(cf)$ , through which the bird has flown since its wing root left the upstream edge of the field of view. Also, the convection time can be used in combination with records of the bird's spanwise location in the wind tunnel to determine the spanwise location on the bird from which the observed wake originates,  $z/b_{semi}$ . The streamwise distance  $\Delta x/c$  and the originating spanwise

position  $z/b_{semi}$  for sequences I through V are shown in Figure 3. The figure indicates that the five sequences of measurements originate from spanwise locations on the bird ranging from  $z/b_{semi} = 0.5$  to  $z/b_{semi} = 0.6$ , and that the measurements have been taken in the range of  $\Delta x/c = 4.4$  to  $\Delta x/c = 6.3$  behind the wing root.

It should be noted that for sequences I through IV, the convection time was calculated using the history of the bird's position from measurements recorded before the sequence. No measurements are available immediately before sequence V, therefore, the position of the bird was assumed constant in the calculation of the convection time.

## RESULTS AND DISCUSSION

### Downstroke to Upstroke: Wake Dynamics

Regions of high spanwise vorticity originating from the downstroke to upstroke transition are identified in sequences I through V. This is confirmed by the net negative circulation and the phase in the wing beat cycle shown by images of the bird  $\Delta\tau$  before the vector field was recorded.

Generally, heaving and pitching airfoil studies focus on vorticity and vorticity dynamics in the wake generated by the unsteady motion. Many studies focusing on the aero/hydrodynamics of animal locomotion describe the wake in terms of vortices as well (Spedding et al., 2003). The definition of a vortex herein is based on the vortex swirling strength,  $\varepsilon$ , defined as the imaginary component of the velocity gradient tensor's eigenvalue (Jeong and Hussain, 1994).

A portion of sequence II is presented in Figure 4 as a sample passage of a strong negative vorticity. A threshold value of  $\varepsilon c/U_\infty = 0.7$  is used as a cut off for vortex identification. Contours of  $\varepsilon c/U_\infty = 0.7$  are plotted over the instantaneous vorticity field in thick, dashed, black lines. The instantaneous velocity field, with the field's spatial average velocity vector removed (i.e., a Galilean decomposition) is shown in the figure as well. As can be seen in the sequence, in which vector fields are offset in time by  $0.02\tau$ , there are several vortices convecting through the field, all with negative circulation. In sequence II, as well as all other sequences, the strongest and largest vortex is upstream of a trail of smaller vortices. The cores of these vortices are at times connected by regions of negative vorticity. This trail of vortices has been related to the bound vortex on the outer part wing during the downstroke to upstroke transition in computational simulations (Ruck and Oertel, 2010). In the simulation, the small structures are attributed to a vortex sheet detaching from the wing.

In the particular case of sequence II, there appears to be two relatively strong vortices in close proximity to one another, visible by both above-threshold levels in swirling strength and peaks in negative vorticity. Although sequence I is at virtually the same location in the flow as sequence II (Figure 3), sequence I shows only one relatively strong vortex

in the presence of smaller vortices further downstream. This is seen in the other sequences as well. The two vortices seen in sequence II are similar to the downstroke stopping vortex and the upstroke starting vortex shown in the simulations of Ruck and Oertel (2010). The model in the simulation was flying with a reduced frequency of 0.34. This is almost twice that of the reduced frequency of the bird in this experiment (0.18). The sinusoidal variation of wing pitch and roll in the simulation, however, produces peak pitch and roll rates which are not necessarily representative of the wing motion of the bird in the present study or birds in general. The lack of perfect dynamic similarity could mean similar wing pitch and roll rates despite different values of the reduced frequency.

### Wake Evolution

Sets I through V are realizations of vorticity shed from the same phase of the wing beat cycle, the downstroke to upstroke transition, originating from a narrow range of spanwise positions in the wake (Figure 3). By tracking properties of the spanwise vorticity over a range of streamwise positions, it is possible to gain insight into the vortex dynamics in the wake. The properties considered herein include circulation of all vorticity (total circulation), vortex circulation, peak vorticity and the vortex core diameter.

Figure 5 summarizes vorticity as a function of streamwise position in sequences I through V. The figure distinguishes between properties of all vorticity in the  $2c$  by  $2c$  field of view, (red), properties of the vortex having the highest swirling strength (black), and all other vortices satisfying the threshold value for identification,  $\varepsilon c/U_\infty=0.7$  (blue). Dashed lines connect peak values of the entire field, and the progression of the strongest vortex of each sequence.

In Figure 5a, the normalized circulations of the entire field of view and of the individual vortices are plotted. Circulation,  $\Gamma$ , has been calculated by numerical integration of the vorticity either over the entire field of view, or, exclusively over regions defined as a 'vortex'. Generally, the normalized circulation,  $\Gamma/(U_\infty c)$ , in the field has peak values of -0.49 to -0.65. The normalized circulation of the strongest vortices have values ranging from -0.04 to -0.25. It should be noted that the extent of this range is due to the two strong vortices observed in sequence II (Figure 3). If the circulation in these two vortex cores were added together, treating the two cores as the one large core seen in the other sequences, the range of  $\Gamma/(U_\infty c)$  would be reduced to approximately -0.12 to -0.25. Figure 5a indicates that at all streamwise locations, 4.8 to 7.1 chords downstream of the wing root, the vortices contain only a fraction of the total vorticity in the field. The plot does not show a trend of changing total circulation in the field, or a change in the proportion of this circulation in the vortices. The generally non-changing total circulation in the field of view indicates that the same amount of vorticity is created from the downstroke to upstroke transition in each sequence of data. Due to the relationship between the circulation in the wake and the kinematics of the bird, this indicates that the flow observed in each sequence is generated from similar movements of the bird (Blondeaux et al., 2005).

Figure 5b shows the peak normalized spanwise vorticity,  $\omega c/U_\infty$ , in the vortices as a function of streamwise position. Peak vorticity in the strongest vortices ranges from -3.4 to -4.8. The peak vorticity in the weaker vortices ranges from -1.5 to -2.8. No trend of increase or decrease of spanwise vorticity is indicated in the plot over the range 4.8 to 7.1 chords. This is especially evident in sequence IV, in which the four recordings of peak vorticity are narrowly centered about an average peak vorticity of -4.3. The constant level of peak spanwise vorticity over the spanwise regions suggests that there is an absence of mechanisms that would otherwise change it. These mechanisms include reorientation of the vortex and compression. Reorientation of the vortex would change the component of vorticity measured (spanwise). Compression, as a result of induced velocity from the tip vortices, would tend to decrease the spanwise vorticity (Dong et al., 2006; Kim and Gharib, 2010).

Figure 5c shows the non-dimensionalized diameter of the vortex cores,  $d_o/c$ , as a function of streamwise position. The core diameters are the diameters of circles having an area equivalent to that of the vortex core. The values of  $d_o/c$  of the strong vortices from each sequence range from 0.12 to 0.35. If the areas of the two strongest vortices in sequence II are combined, however, the range of  $d_o/c$  reduces to 0.2 to 0.35. The plot does not indicate that the core diameters are either increasing or decreasing, however, the trend in each individual sequence is for the core to grow.

### CONCLUSIONS

The present study focuses on the spanwise vorticity shed from the wing during the transition from downstroke to upstroke. Several regions that can be classified as vortices were found, generally with a particularly strong vortex upstream of smaller, weaker ones of the same sense.

Characteristics of the spanwise vorticity have been considered over a range of streamwise positions. Since the focus of the work is limited to the vorticity shed from one particular phase of the wing beat cycle, the streamwise position at which the vorticity is observed can be related to the time it has had to develop. Typically, in the near wake of an unsteady wing, the interaction between the vorticity from the shed bound vortex and the other vorticity in the wake would be responsible for this development (Dong et al., 2006; Kim and Gharib, 2010). This development would manifest itself as changes in the spanwise vorticity shed from the wing.

Results indicate that the characteristics of the vorticity shed from the downstroke to upstroke transition do not change over the streamwise interval of 4.8 to 7.1 chords downstream of the wing root. While the flow is three dimensional, this shows that properties of the vorticity including circulation, circulation within vortex cores, peak vorticity and core diameter are not under significant influence of mechanisms that would cause them to change

## REFERENCES

- Anderson J. M., Streitlien K., Barret D. S., Triantafyllou M. S., 1998, "Oscillating foils of high propulsive efficiency", *Journal of Fluid Mechanics*, Vol. 360, pp. 41-72
- Blondeaux F., Fornarelli F., Guglielmini L., 2005, "Numerical experiments on flapping foils mimicking fish-like locomotion", *Physics of Fluids*, Vol. 17, 113601
- Dong H., Mittal R., Najjar F. M., 2006 "Wake topology and hydrodynamic performance of low-aspect-ratio flapping Foils", *Journal of Fluid Mechanics*, Vol. 566, pp. 309-343
- Hubel T. Y., Tropea C., "The importance of leading edge vortices under simplified flapping flight conditions at the size scale of birds", *The Journal of Experimental Biology*, Vol. 213, pp. 1930-1939
- Jeong J., Hussain F., 1994, "On the identification of a vortex", *Journal of Fluid Mechanics*, Vol. 285, pp. 69-94
- Kim D., Gharib M., 2010, "Experimental study of three-dimensional vortex structures in translating and rotating plates", *Experiments in Fluids*, Vol. 49, pp. 329-339
- Rhozhdestvensky, V., Ryzhov V., 2003, "Aerodynamics of flapping-wing propulsors", *Progress in Aerospace Sciences*, Vol. 39, pp. 585-633
- Ruck S., Oertel H., Jr., 2010, "Fluid-structure interaction simulation of an avian flight model", *The Journal of Experimental Biology*, Vol. 213, pp. 4180-4192
- Spedding G. R., Rósen M., Hedenström A., 2003, "A family of vortex wakes generated by a thrush nightingale in free flight in a wind tunnel over its entire natural range of flight speeds," *The Journal of Experimental Biology*, Vol. 206, pp. 2313-2344
- Taylor G.K., Nudds L.R., Thomas A.L.R., 2003, "Flying and swimming animals cruise at a Strouhal number tuned for high power efficiency", *Nature*, Vol. 425 pp. 707-711
- Taylor Z. J., Gurka R., Kopp G. A., Liberzon A., 2010, "Long-duration time-resolved PIV to study unsteady aerodynamics," *IEEE Transactions on Instrumentation and Measurement*, Vol. 59, pp. 3262-3269
- von Ellenrieder K. D., Parker K., Soria J., 2008, "Fluid mechanics of flapping flight," *Experimental Thermal and Fluid Science*, Vol. 32 pp. 1578-1589

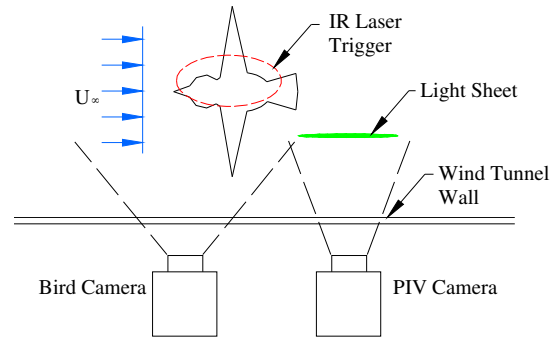


Figure 1. A schematic plan view of the experimental setup.

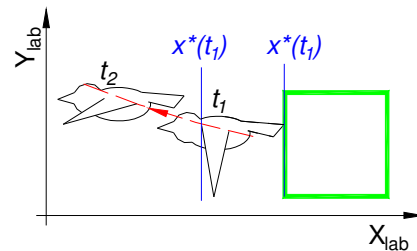


Figure 2. A schematic view of the bird interacting with the frame of reference at  $t_1$  and later triggering the PIV laser at  $t_2$ .

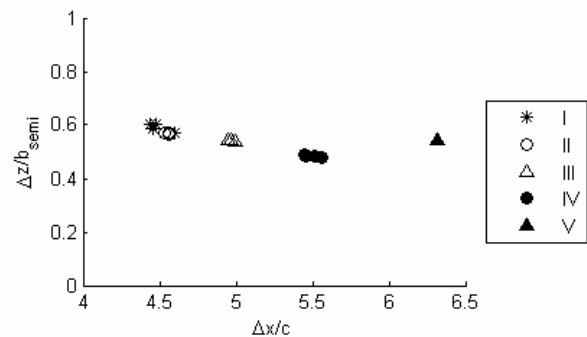


Figure 3. A summary of the bird's streamwise position and the spanwise position from which the wake originates.

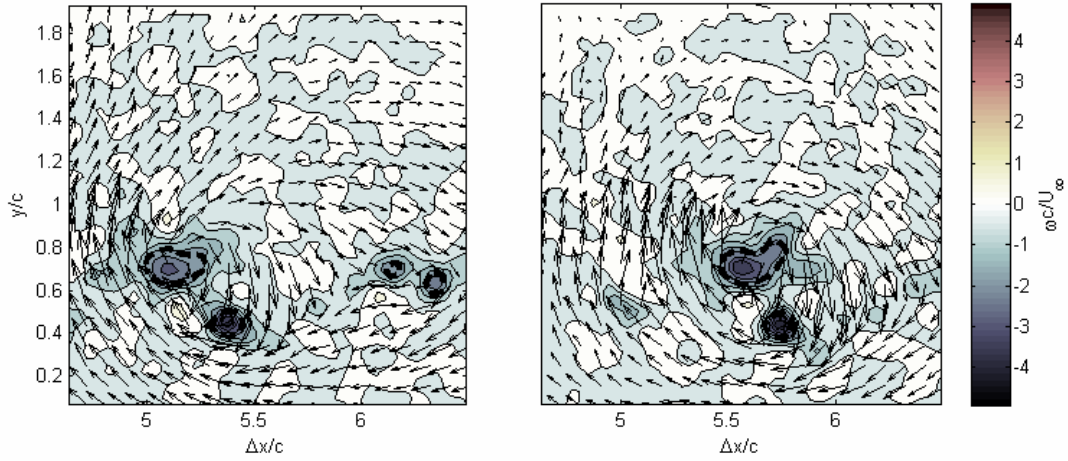


Figure 4. The passage of a region of strong negative spanwise vorticity seen in sequence II, originating from the downstroke to upstroke transition of the wing.  $z/b_{semi} = 0.6$ . Regions of  $\epsilon c/U_\infty = 0.7$  are indicated by thick black contours. The plots are separated by a time interval of  $0.02\tau$ .

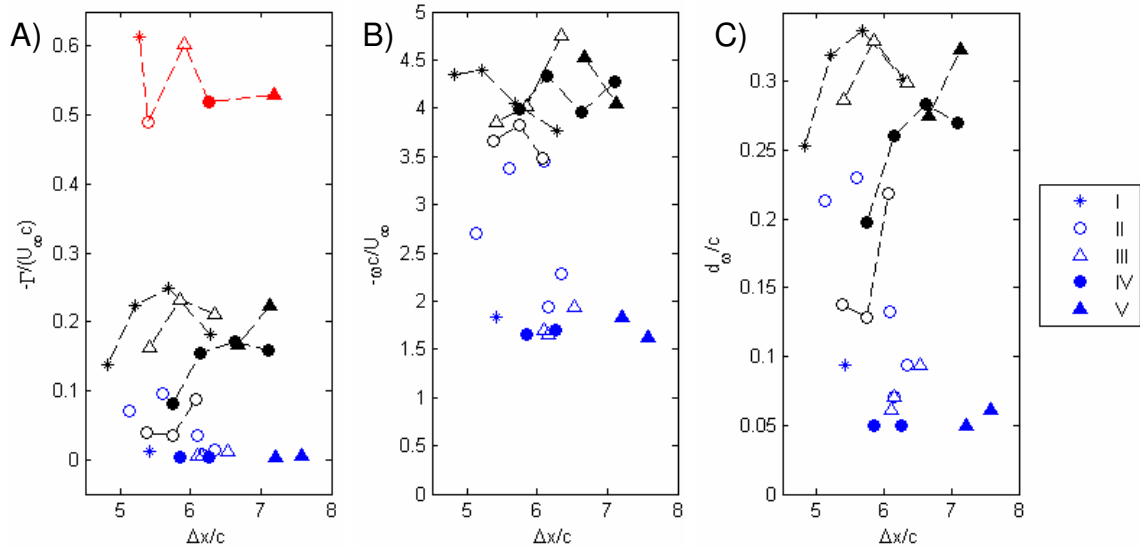


Figure 5. Properties of the vorticity and vortices in the wake as a function of streamwise position. Smaller eddies are shown in blue. In A) the circulation of the vortices (black) and the peak total circulation in each set (red) are plotted. In B), the peak vorticity in all vortices found is plotted. In C) the core diameter is plotted.